Triangular Current Mode Control for High-Frequency Inverter Operation without Bottom-Current Detection

Yuki Mashita[1]*, Rintaro Kusui[1], Takumi Iwamoto[1], Kodai Nishikawa[1], Hiroki Watanabe[1], Jun-ichi Itoh[1]
1 Department of Electrical, Electronics and Information Engineering, Nagaoka University of Technology, Niigata, Japan
*s255025@stn.nagaokaut.ac.jp

***Abstract*—Increasing the switching frequency is an effective approach to improving the power density of power converters. However, in high-frequency operation, accurate bottom-current detection becomes difficult due to bandwidth limitations caused by parasitic components and peripheral circuits. This paper proposes a triangular current mode (TCM) control method that eliminates the need for bottom-current detection by determining the switching frequency from the current command using a conventional PI controller. The proposed approach regulates the average inverter output current while maintaining the bottom current required for zero-voltage switching (ZVS). The effectiveness of the method is demonstrated through transient response measurements and rated operation tests. Experimental results show that the bottom current is maintained above the minimum level required to achieve ZVS under most operating conditions in both totem-pole and full-bridge modes, achieving low current distortion and efficiencies of 94.6% and 95.3%, respectively.**

Keywords—Triangular Current Mode, Zero Voltage Switching, Single-Phase Inverter, Variable Frequency

I. Introduction

The rising demand for energy efficiency has highlighted the need for further advancements in power electronics technology [1]-[3]. Efficient power converters are essential for improving overall energy efficiency. However, conventional power converters require extensive specialized design efforts, including circuit design, thermal management, noise reduction, and software development. As a result, development cycles are often lengthy due to the complexity of conventional power converter design. To address this, the Strategic Innovation Promotion Program (SIP) of the Cabinet Office is promoting research and development on the Universal Smart Power Module (USPM) [4],[5]. The USPM is an integrated package that includes all essential components of a power converter, such as the main circuit, gate driver, and controller. By selecting and combining the necessary modules, users can build their desired power converter, significantly shortening development time. To enable wider adoption of USPMs, further enhancements in converter power density are necessary.

Higher switching frequency helps increase power density in power converters. Raising the switching frequency allows for smaller passive components, boosting power density. However, higher frequency also leads to increased switching losses, which require larger cooling systems. This creates a practical limit on how much power density can be improved. To address this issue, soft switching based on the triangular current mode (TCM) has been proposed [6]. Conventional TCM control sets the switching timing based on the bottom current detected by a shunt resistor [7],[8]. Other approaches also rely on bottom-current detection using current sensors [9], [10]. In addition, Hybrid mode control methods maintain ZVS by utilizing current information [11]. However, at high switching frequencies in the MHz range, parasitic components and peripheral circuits limit bandwidth, making high-speed current detection challenging. To address these issues, this paper aims to realize TCM control without bottom-current detection under high-frequency operation while suppressing instability near the zero-crossing point.

This paper proposes a TCM control method that eliminates the need for bottom-current detection by applying variable switching frequency to a conventional PI controller. The switching frequency is determined from the current command to maintain a constant bottom current. A key advantage of the proposed method is that it enables TCM control at high switching frequency, where shunt-resistor current sensing is not feasible. The main contribution of this paper is a control strategy that avoids computational instability in the switching-frequency calculation near the zero-crossing point. The proposed method prevents division by zero and enables stable variable-frequency operation without direct bottom-current detection. Furthermore, transient response measurements and rated operation tests indicate the effectiveness of the proposed method. Control characteristics are evaluated through step response testing, and two modulation methods are assessed for total harmonic distortion (THD). Experimental results show that the bottom current remains above the minimum level required to achieve ZVS under most operating conditions in both totem-pole and full-bridge modes, enabling low current distortion and achieving efficiencies of 94.6% and 95.3%, respectively.

II. Triangular Current Mode Control Without Bottom-Current Detection

A. Circuit Configuration

Fig. 1 shows the circuit diagram of a single-phase inverter connected to an LCL filter. In TCM operation, a large current ripple occurs in the grid-tied inductor. However, the ripple in the filter inductor current is sufficiently suppressed. In this study, the filter inductor current is used as the feedback signal.

B. Block Diagram of the Proposed Control Method

Fig. 2 shows the control block diagram of the proposed method. The proposed method achieves TCM operation without directly detecting the bottom current. The proposed

method assumes operation at a high switching frequency of several MHz. Under this condition, high-speed current detection using a shunt resistor is not practical. Therefore, the proposed method calculates the switching frequency based on the current command, the filter capacitor voltage, and the bottom current command required for ZVS instead of directly detecting the bottom current. The error caused by output current variations or parameter mismatches is compensated by adjusting the duty ratio through PI control. In contrast, the feedback control uses the filter inductor current whose ripple is sufficiently suppressed. The detected filter inductor current is compared with the current command, and the command voltage of the grid-tied inductor is generated by a PI compensator. A triangular carrier wave is generated using the calculated switching frequency. The switching signal is generated by comparing the triangular carrier with the duty command from the comparator.

C. Derivation of the Switching Frequency

Fig. 3 shows the switching patterns while the inverter outputs a positive voltage. This paper compares the totem-pole mode, in which only one leg is switched at high frequency, with the full-bridge mode, in which both legs are switched at high frequency. In the totem-pole mode shown in Fig. 3(a), one leg with the upper switch S_1 remains in the on state during the positive output period. The other leg is switched according to the duty command d_2. When S_3 is on, the converter output voltage V_{conv} becomes zero. When S_3 is off, V_{conv} becomes equal to the DC input voltage V_{in}. The interval in which the output voltage becomes zero is defined as the off period t_{off}. The interval in which the output voltage is equal to V_{in} is defined as the on period t_{on}. These periods are expressed as

$$t_{on} = \frac{1-d_2}{f_{sw}} \tag{1}$$

$$t_{off} = \frac{d_2}{f_{sw}} \tag{2}$$

where f_{sw} is the switching frequency. To achieve TCM operation, the ripple ratio of the grid-tied inductor current must exceed 200%. Thus, the current change and the average current are calculated. Assuming that the current variation during one switching cycle is ΔI_L and that the bottom current I_{bot} is constant, the current variation ΔI_L is expressed as

$$\triangle I_L = \frac{V_{in} - |V_c|}{L} t_{on} = \frac{V_{in} - |V_c|}{f_{sw} L} \frac{|V_c|}{V_{in}} \tag{3}$$

$$\triangle I_L = 2(|i_{ave}| + I_{bot}) \tag{4}$$

where V_c is the filter capacitor voltage, i_{ave} is the average current. From (3) and (4), the switching frequency is determined by (5). Therefore, the desired bottom current is achieved without direct current detection.

$$f_{sw} = \frac{|V_c|(V_{in} - |V_c|)}{2LV_{in}(|i_{ave}| + I_{bot})} \tag{5}$$

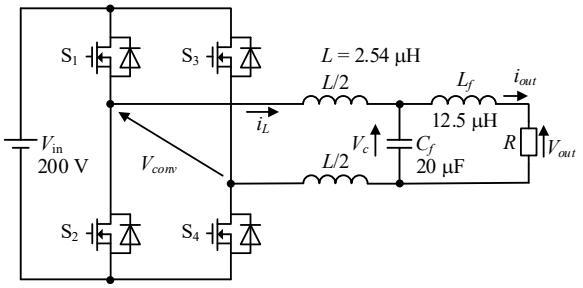

Fig. 1 Circuit diagram and parameters of full-bridge inverter.

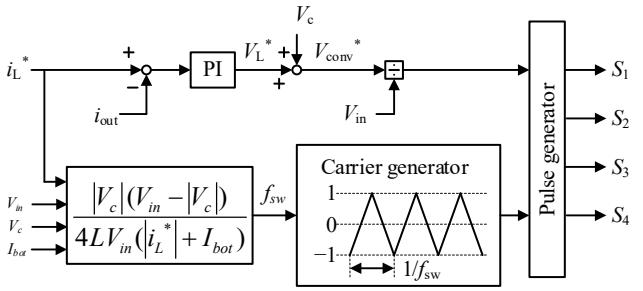

Fig. 2. Block diagram of proposed current controller with TCM

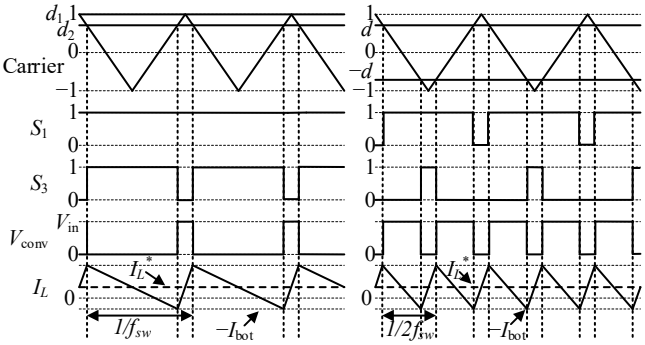

(a) totem-pole mode (b) full-bridge mode

Fig. 3 Switching pattern of unipolar modulation.

Table. 1. Experiment Parameter with TCM operation

Parameters	Symbol	Value
Input voltage	V_{in}	200 V
Rated output power	P_{rated}	1 kW
Grid frequency	f_g	50 Hz
Maximum switching frequency	f_{sw_max}	Full bridge: 600 kHz Totem pole: 1.2 MHz
Minimum switching frequency	f_{sw_min}	Full bridge: 200 kHz Totem pole: 400 kHz
Bottom current	I_{bot}	2 A
Resistor	R	9.4 Ω
Grid-tied inductance	L	2.54 μH
Filter inductance	L_f	12.5 μH
Filter capacitance	C_f	20 μF
Rated impedance	Z_n	10 Ω
Normalized proportional gain	$K_{p\text{-}pu}$	0.03 (K_p/Z_n)
Integration time	T_i	50 μs

On the other hand, in the full-bridge mode, the duty command d is applied with reversed polarity to generate the gate signals of the two legs. The converter output voltage V_{conv} becomes V_{in}. As in the totem-pole mode, the on period t_{on} and the off period t_{off} are defined. These durations are expressed as

$$t_{on} = \frac{2d-1}{2f_{sw}} \tag{6}$$

$$t_{off} = \frac{1-d}{f_{sw}} \tag{7}$$

Using a derivation similar to that of the totem-pole mode, the current variation ΔI_L is expressed as

$$\triangle I_L = \frac{V_{in} - |V_c|}{L} t_{on} = 2 \frac{V_{in} - |V_c|}{f_{sw} L} \frac{|V_c|}{V_{in}} \tag{8}$$

$$\triangle I_L = 2(|i_{ave}| + I_{bot}) \tag{9}$$

From (8) and (9), the switching frequency is obtained as (10). Therefore, the desired bottom current is achieved without direct current detection.

$$f_{sw} = \frac{|V_c|(V_{in} - |V_c|)}{4LV_{in}(|i_{ave}| + I_{bot})} \tag{10}$$

In the full-bridge mode, the output voltage frequency becomes twice that in the totem-pole mode. Thus, to maintain the same current ripple, the value of the grid-tied inductor is reduced to half. Furthermore, according to (5) and (10), when the filter capacitor voltage V_c is low, the switching frequency approaches zero. In such cases, the switching frequency is limited to ensure adequate control of the output voltage.

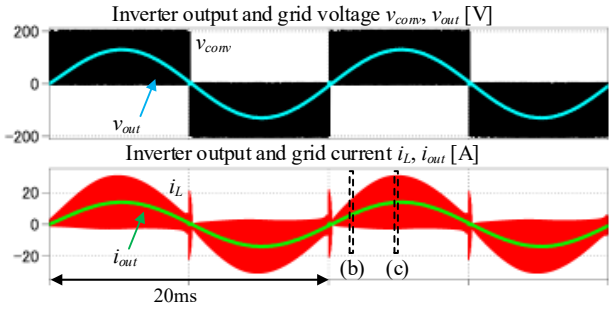

(a) Output current waveform at 50 Hz, with a THD of 0.96%.

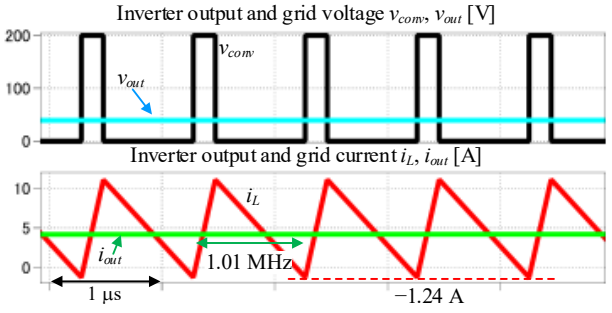

(b) Enlarged waveform at a grid-tied inductor current frequency of approximately 1.01 MHz, showing variable-frequency operation (switching frequency: 400–1.2 MHz range).

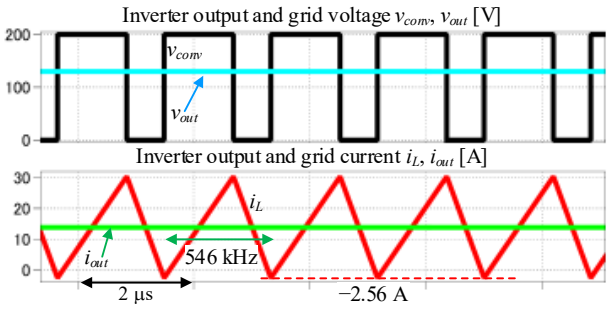

(c) Enlarged waveform at a grid-tied inductor current frequency of approximately 546 kHz, showing variable-frequency operation (switching frequency: 400–1.2 MHz range).

Fig. 4 Waveforms during rated-operation simulations of the TCM inverter in the totem-pole mode.

III. Simulation Results

A. Operation of the Proposed Method

Table 1 shows the simulation and experimental conditions. This section compares the THD, operating frequency and bottom current of the totem-pole and full-bridge modes. It also verifies whether the bottom current can be maintained at a constant value using the proposed method. The inductance is set to 2.54 µH in both the totem-pole and full-bridge modes. The DC input voltage is 200 V, and the current command is 10 A. The switching frequency ranges from 400 kHz to 1.2 MHz in the totem-pole mode and from 200 kHz to 600 kHz in the full-bridge mode. These minimum switching frequencies correspond to the operating point at which both the voltage and current reach their maximum values. The proportional gain is normalized by the rated impedance. As a result, the normalized proportional gain is set to 0.03. The integral time is set to 50 µs.

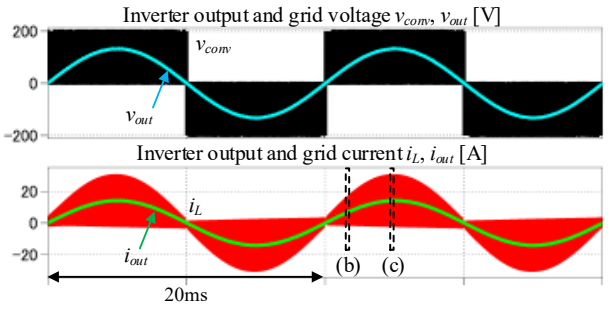

(a) Output current waveform at 50 Hz, with a THD of less than 0.5%.

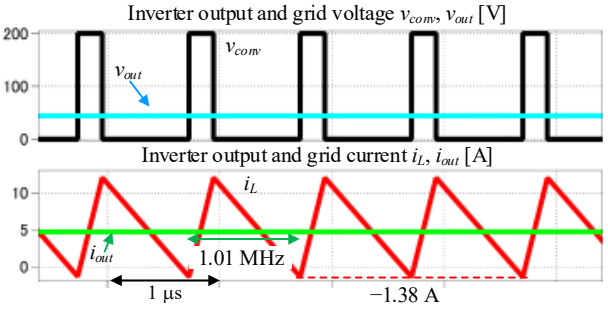

(b) Enlarged waveform at a grid-tied inductor current frequency of approximately 1.01 MHz, confirming variable-frequency operation (switching frequency: 200–600 kHz range).

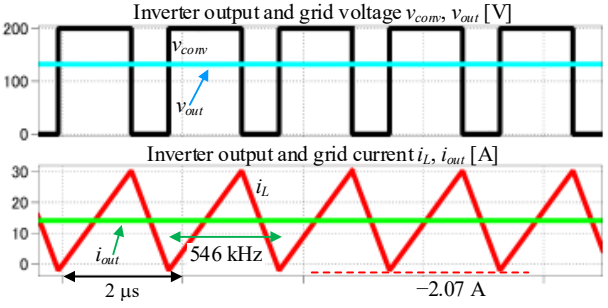

(c) Enlarged waveform at a grid-tied inductor current frequency of approximately 546 kHz, confirming variable-frequency operation (switching frequency: 200–600 kHz range).

Fig. 5. Waveforms during rated-operation simulations of the TCM inverter in the full-bridge mode.

Figs. 4 and 5 show the simulation results of the proposed method in the totem-pole and full-bridge modes. Figs. 4(a) and 5(a) show the output waveforms at a grid frequency of 50 Hz. At the rated output power of 1 kW, the total harmonic distortion (THD) is 0.96% in the totem-pole mode and less than 0.5% in the full-bridge mode. Fig. 4(a) shows current distortion near the zero-crossing point. This distortion occurs when the current polarity changes. At this moment, the upper and lower switches of one leg are commutated. Because of the delay in the feedback control, the duty ratio temporarily exceeds 1 or −1. As a result, the PWM signal becomes saturated and the switching operation stops for a short period. This non-switching interval causes the current distortion.

Figs. 4(b), (c) and 5(b), (c) show the enlarged waveforms. Figs. 4(b) and 5(b) show the region near the maximum value (1.01 MHz) in the totem-pole and full-bridge modes , respectively. Note that the equivalent switching frequency of the grid-tied inductor current in the full-bridge mode becomes twice the switching frequency because both legs are switched. Figs. 4(c) and 5(c) show the region near the minimum switching frequency (546 kHz) in the totem-pole and full-bridge modes , respectively. The converter operates with a variable switching frequency and the switching frequency varies depending on the load current. This behavior is caused by the control objective of maintaining a constant bottom current. The grid-tied inductor current reaches negative values, confirming TCM operation under variable switching frequency. Therefore, an appropriate switching frequency that enables TCM operation is applied to this converter. In addition, under variable switching frequency operation, the bottom current becomes 1.24 A in the totem-pole mode and 1.38 A in the full-bridge mode at the point of the maximum switching frequency. Near the peak current region, the bottom current is 2.56 A in the totem-pole mode and 2.07 A in the full-bridge mode. These values deviate from the design value of 2 A. The main reason is the use of an estimated value for the capacitor voltage V_c. The detected value is difficult to use for the following reasons. Under this condition, the switching frequency differs from the sampling frequency. Aliasing occurs due to the difference between the switching frequency and the sampling frequency. Therefore, it is difficult to directly use the detected value. In this study, the estimated capacitor voltage is applied as a feedforward signal.

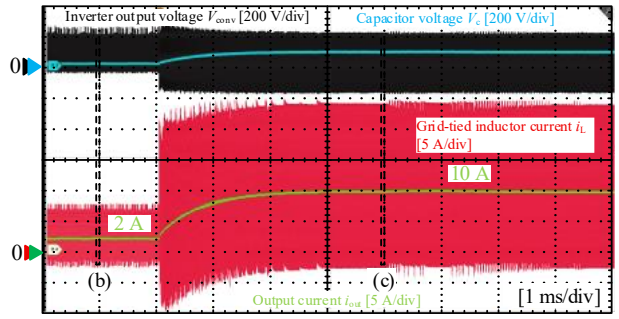

(a) Step response of the inductor current for a current command change from 2 A to 10 A.

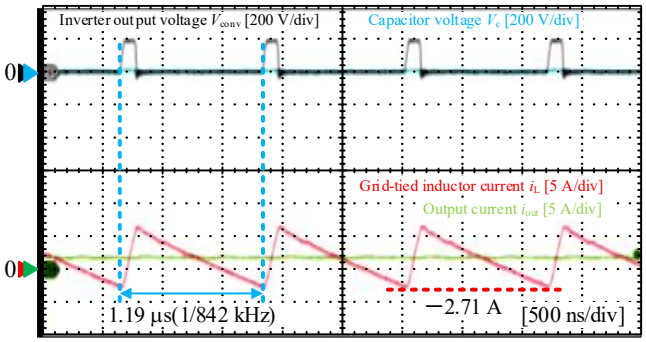

(b) Enlarged waveform showing the inductor current tracking the 2 A command.

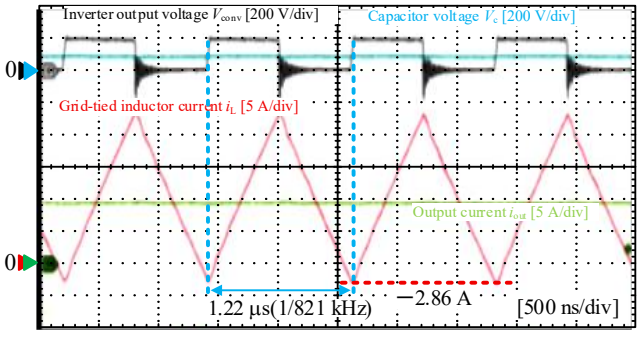

(c) Enlarged waveform showing the inductor current tracking the 10 A command.

Fig. 6. Transient response of the inductor current in the totem-pole mode

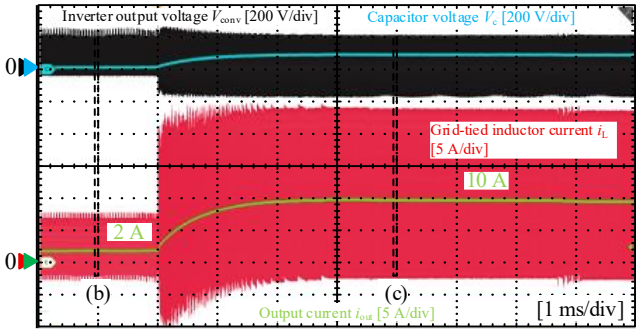

(a) Step response of the inductor current for a current command change from 2 A to 10 A.

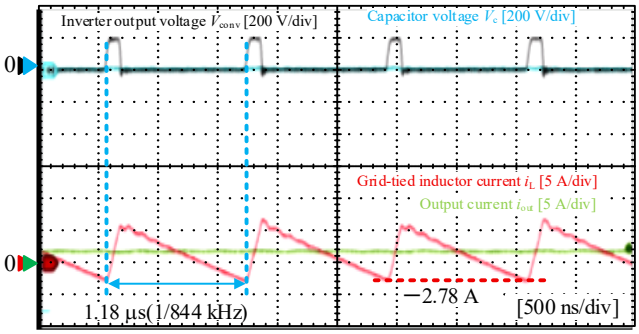

(b) Enlarged waveform showing the inductor current tracking the 2 A command.

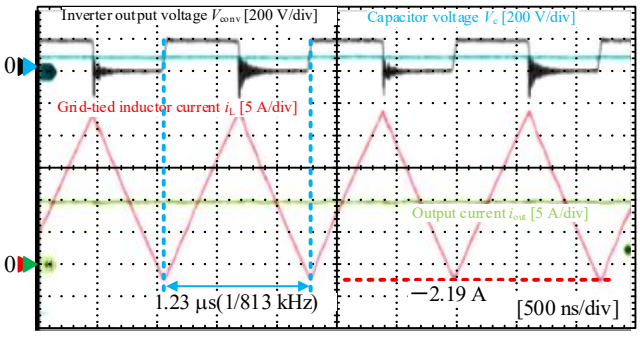

(c) Enlarged waveform showing the inductor current tracking the 10 A command.

Fig. 7. Transient response of the inductor current in the full-bridge mode

IV. Experimental Results

A. Load Step Response

An experiment is conducted with the same parameters as in the simulation in Section III. Fig. 6(a) shows the step response waveform for the totem-pole mode, and Fig. 7(a) shows that for the full-bridge mode. The current command is stepped from 2 A to 10 A. The variable switching frequency is calculated using the estimated capacitor voltage. Therefore, the bottom current exceeds the command during the transient period because of the difference between the estimated value and the actual value. However, in the steady state, the bottom current approaches the command. In addition, the bottom current does not become smaller than the design value even during the transient state. When the bottom current is equal to or greater than the design value, sufficient energy is ensured to discharge the device capacitance, thereby achieving ZVS. Consequently, the bottom current during the transient period does not cause a problem.

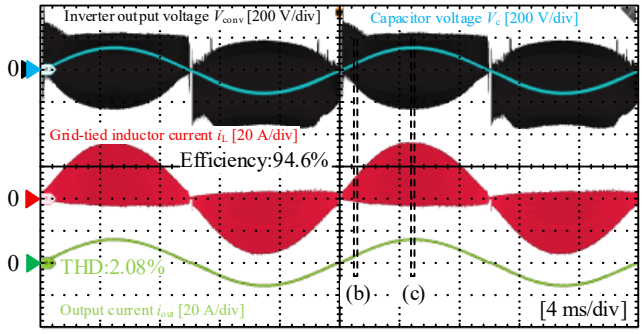

(a) Output current waveform at 50 Hz, with an efficiency of 94.6% and a THD of 2.08%.

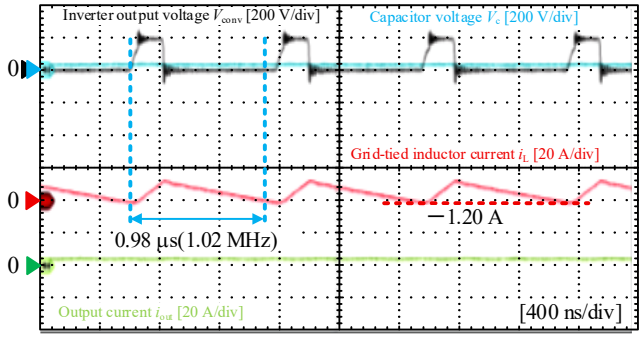

(b) Enlarged waveform at a grid-tied inductor current frequency of approximately 1.01 MHz, showing variable-frequency operation (switching frequency: 400–1.2 MHz range).

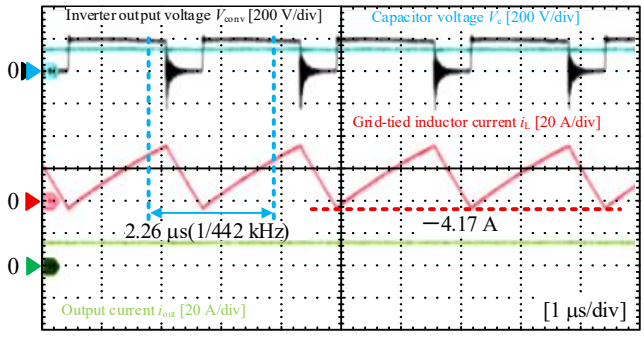

(c) Enlarged waveform at a grid-tied inductor current frequency of approximately 442 kHz, showing variable-frequency operation (switching frequency: 400–1.2 MHz range).

Fig. 8. Waveforms during rated-operation tests of the TCM inverter in the totem-pole mode.

Figs. 6(b), (c), and 7(b), (c) confirm that the current value accurately follows the command, verifying the proper operation of the PI control. Furthermore, the bottom current is generally controlled above the minimum level required to achieve ZVS, demonstrating that the proposed method stably maintains the current required for ZVS.

B. Operation of the Proposed Method

Figs. 8(a) and 9(a) show the output current waveforms. The bottom value of the grid-tied inductor current remains above the minimum level required to achieve ZVS under most operating conditions for both modulation schemes. The switching frequency varies based on the current command and the capacitor voltage in the proposed method. As a result, the bottom current is generally controlled even when the operating conditions vary. Figs. 8(b) and 8(c) show enlarged waveforms for the totem-pole mode, with switching frequencies of 1.02 MHz and 1.00 MHz, respectively. In contrast, Figs. 9(b) and 9(c) show enlarged waveforms for the full-bridge mode, with switching frequencies of 442 kHz and

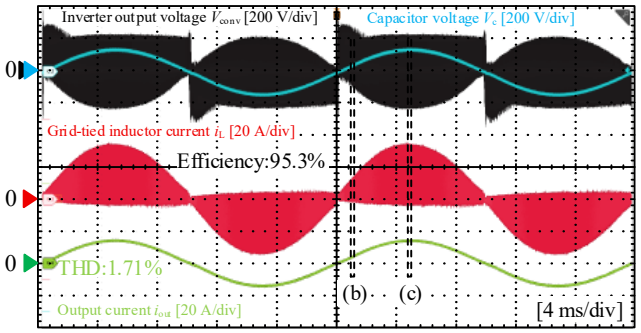

(a) Output current waveform at 50 Hz, with an efficiency of 95.3% and a THD of 1.71%.

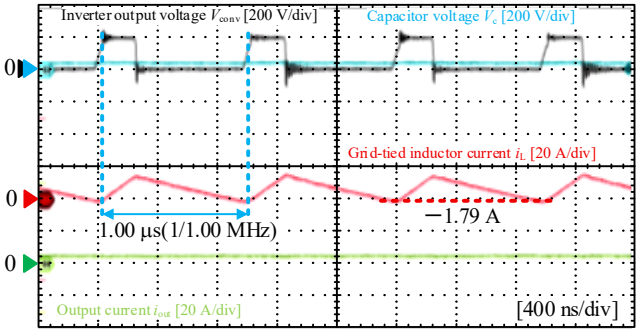

(b) Enlarged waveform at a grid-tied inductor current frequency of approximately 1.00 MHz, confirming variable-frequency operation (switching frequency: 200–600 kHz range).

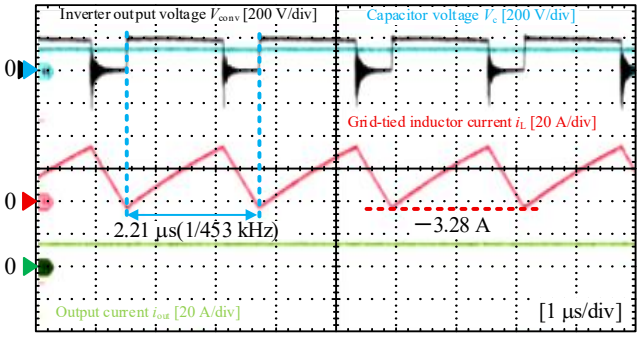

(c) Enlarged waveform at a grid-tied inductor current frequency of approximately 453 kHz, confirming variable-frequency operation (switching frequency: 200–600 kHz range).

Fig. 9. Waveforms during rated-operation tests of the TCM inverter in the full-bridge mode.

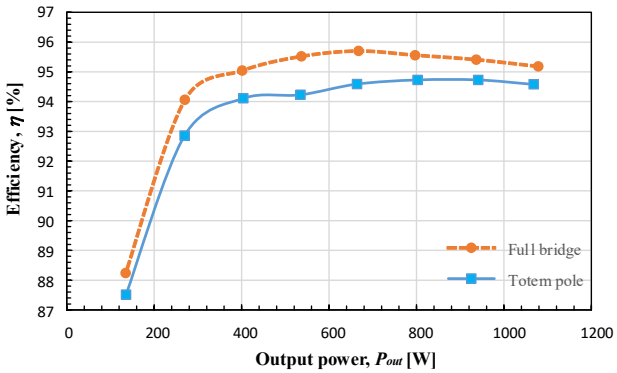

Fig. 10. Measured efficiency curve of TCM operation under a constant output voltage of 100 V and varying load resistance.

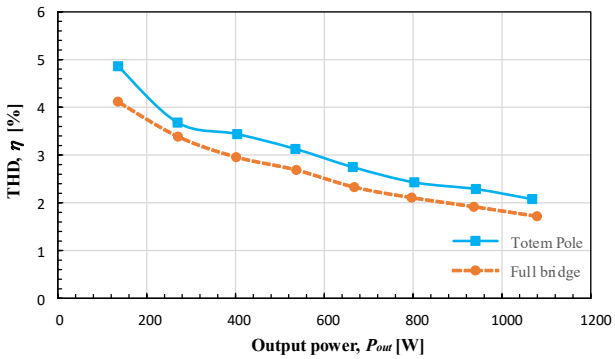

Fig. 11. Measured THD curve of TCM operation under a constant output voltage of 100 V and varying load resistance.

453 kHz, respectively. This variation in switching frequency is caused by the control objective of maintaining the bottom current above the minimum level required for ZVS. When the output voltage is low, the current ripple must be reduced. Therefore, a higher switching frequency is required. Conversely, when the output voltage is high, a larger ripple is allowed. As a result, the switching frequency becomes lower. These results support the conclusion that the proposed method adaptively adjusts the switching frequency to maintain the required bottom current and enables stable variable-frequency operation in both modulation schemes.

As shown in Figs. 8(b), 8(c) and 9(b), 9(c), the bottom current varies depending on the operating conditions, such as the output voltage and current, and deviates from the design value of 2 A. One of the main causes is the variation in the inductance of the grid-tied inductor, which depends on the magnitude of the applied current. Changes in the applied current alter the permeability of the magnetic material, resulting in a corresponding change in inductance. Since the switching frequency is calculated assuming a constant inductance, this mismatch leads to errors in the frequency calculation, resulting in deviations in the bottom current.

The THD of the filter inductor current is 2.08% in the totem-pole mode and 1.71% in the full-bridge mode. Near the zero-crossing point, the inductor current decreases, and the switching frequency reaches its minimum. Under these conditions, the current polarity changes and distortion tends to occur. However, both the totem-pole and full-bridge modes operate with a THD of less than 5%. From the comparison between the totem-pole and full-bridge modes, the full-bridge mode shows superior performance under the tested conditions in terms of THD and efficiency, mainly due to the absence of PWM saturation near the zero-crossing point.

In addition, ZVS is suggested from the rising waveform of the inverter voltage. From Figs. 8(c) and 9(c), the inverter voltage rises gradually before the turn-on transition, suggesting that ZVS is likely achieved under these operating conditions. However, a more rigorous verification based on the device voltage and gate signal would be required for a conclusive demonstration.

C. *Efficiency Evaluation*

Fig. 10 shows the conversion efficiency over the output power range of 0.1-1.1 kW. The maximum efficiency is 94.6% for the totem-pole mode and 95.3% for the full-bridge mode at 0.8 kW and 0.7 kW output power, respectively. Although ideal ZVS eliminates switching losses, practical losses remain due to parasitic resistances in the discharge path of the output capacitance and carrier recombination within the semiconductor device. Efficiency decreases as output power decreases. As the output power decreases, the command also decreases, resulting in lower conduction losses, which are proportional to the square of the current. However, losses independent of the current, such as switching loss, remain nearly constant. Consequently, at low output power, the proportion of these losses in the total losses increases, reducing efficiency.

D. *THD Evaluation*

Fig. 11 shows the filter inductor current THD over the output power range from 0.1 kW to 1.1 kW. The minimum THD is 2.08% for the totem-pole mode and 1.71% for the full-bridge mode at 1.1kW output power. The THD in the full-bridge mode is lower than that in the totem-pole mode. This is because the switching operation stops near the zero-crossing point in the totem-pole mode, which causes current distortion. At the zero-crossing point, the duty ratio of one leg changes abruptly in the totem-pole mode due to the polarity reversal of the current. At this moment, the duty ratio exceeds its limit because of the delay in the current response. As a result, the PWM signal becomes saturated and the switching operation temporarily stops. In contrast, in the full-bridge mode, the duty ratio does not change abruptly near the zero-crossing point. Therefore, PWM saturation does not occur, and the THD becomes lower.

V. Conclusion

This paper proposed a triangular current mode (TCM) control method that eliminates the need for bottom-current detection. The method employs a conventional PI controller and determines the switching frequency based on the current command. As a result, the bottom current was maintained at a constant value without bottom-current detection. The effectiveness of the proposed method was demonstrated through transient response measurements and rated operation tests. Experimental results showed that the bottom current remained above the minimum level required to achieve ZVS under most operating conditions in both totem-pole and full-bridge modes, reliably ensuring the current required for ZVS while achieving low current distortion and efficiencies of 94.6% and 95.3%, respectively. The proposed method enables TCM operation while maintaining ZVS, eliminating the need for bottom-current detection. This feature makes the proposed method suitable for power converters that require high power density. Future work includes developing control techniques to improve disturbance rejection further and reduce current distortion.

ACKNOWLEDGMENT

This work was supported by Council for Science, Technology and Innovation(CSTI), Cross-ministerial Strategic Innovation Promotion Program (SIP), the 3rd period of SIP “ Smart energy management system ” Grant Number JPJ012207 (Funding agency: JST).

REFERENCES

[1] K. Tomida, K. Natori, J. Xu, N. Shimosato, and Y. Sato, “A novel control method to improve efficiency in wide output voltage range for bidirectional isolated three-phase AC/DC converter based on matrix converter,” IEEJ J. Ind. Appl., vol. 13, no. 1, pp. 17–23, 2024.

[2] A. Kawamura, Y. Tsuruta, and H. Obara, “Over 99.7% efficiency at 100 kW DC–DC power conversion using a 3.3 kV SiC device and discussion on device dv/dt estimation,” IEEJ J. Ind. Appl., vol. 13, no. 4, pp. 426–436, 2024.

[3] N. Fujishima, “Technical trends of SiC power semiconductor devices and their applications in power electronics,” IEEJ J. Ind. Appl., vol. 13, no. 4, pp. 372–378, 2024.

[4] D. Hiroe, T. Yabuki, T. Hamauzu, T. Shimono, A. Kawamura, and T. Yokoyama, “Experimental verification of 10 MHz multi-sampling deadbeat control for PMLSM drive system using USPM controller,” IEEJ J. Ind. Appl., vol. 15, no. 2, pp. 230–239, 2026.

[5] H. Watanabe, K. Yamanokuchi, Y. Ikeda, Y. Takahashi, and J.-i. Itoh, “Universal smart power module (USPM) for carbon neutral society,” IEEE Trans. Ind. Appl., vol. 60, no. 2, pp. 3411–3417, 2024.

[6] Y. Shen, H. Wang, Z. Shen, Y. Yang, and F. Blaabjerg, “A 1-MHz series resonant DC–DC converter with a dual-mode rectifier for PV microinverters,” IEEE Trans. Power Electron., vol. 34, no. 7, pp. 6544–6564, 2019.

[7] S. Ohn, N. Hayani, R. Burgos, and D. Boroyevich, “A simplified digital closed-loop current control of three-phase PV inverter operating in triangular conduction mode,” in Proc. Int. Conf. Power Electron. (ICPE), pp. 2027–2033, 2019.

[8] C. H. Park, D. Y. Kim, H. B. Yeon, Y. D. Son, and J. M. Kim, “A current reconstruction strategy following the operation area in a 1-shunt inverter system,” Energies, vol. 12, no. 8, p. 1423, 2019.

[9] C. Marxgut, F. Krismer, D. Bortis, and J. W. Kolar, “Ultraflat interleaved triangular current mode (TCM) single-phase PFC rectifier,” IEEE Trans. Power Electron., vol. 29, no. 2, pp. 873–882, 2014.

[10] C. Marxgut, J. Biela, and J. W. Kolar, “Interleaved triangular current mode (TCM) resonant transition single-phase PFC rectifier with high efficiency and high power density,” in Proc. Int. Power Electron. Conf., pp. 1725–1732, 2010.

[11] Y. Jiang, Y. Shen, L. Shillaber, B. Hu, C. Jiang, and T. Long, “Hybrid-mode adaptive zero-voltage switching for single-phase DC–AC conversion with paralleled SiC MOSFETs,” IEEE Trans. Power Electron., vol. 37, no. 12, pp. 14067–14081, 2022.